Journal of Photochemistry and Photobiology A: Chemistry 205 (2009) 70–76

Contents lists available at ScienceDirect

Journal of Photochemistry and Photobiology A: Chemistry

journal homepage: www.elsevier.com/locate/jphotochem

A simple route towards low-temperature processing of nanoporous thin films using UV-irradiation: Application for dye solar cells

Zoe Tebby[a], Odile Babot[a], Dominique Michau[b], Lionel Hirsch[c], Luis Carlos[d], Thierry Toupance[a,*]

[a] University of Bordeaux 1, Institut des Sciences Moléculaires, Groupe Matériaux UMR 5255 CNRS, 351 Cours de la Libération, F-33405 Talence Cedex, France
[b] Institut de Chimie de la Matière Condensée de Bordeaux, UPR 9048 CNRS, Château Brivazac, Avenue du Docteur A. Schweitzer, F-33608 Pessac Cedex, France
[c] Laboratoire de l'Intégration du Matériau au Système, UMR 5218 CNRS, ENSCPB, 16 Avenue Pey-Berland, 33607 Pessac Cedex, France
[d] Departemento de Fisica and CICECO, Universidade de Aveiro, 3810-193 Aveiro, Portugal

ARTICLE INFO

Article history:
Received 20 January 2009
Received in revised form 23 March 2009
Accepted 26 March 2009
Available online 5 April 2009

Keywords:
Titanium dioxide
Tin dioxide
UV-processing
Photosensitization
Dye solar cells
Flexible substrates

ABSTRACT

Fabrication of anatase TiO_2 porous films at low temperature was achieved by a very simple, straightforward and cheap method involving the connection of oxide particles by UV-irradiation in air. The novelty of the method relies on the direct UV-irradiation of oxide nanoparticles, without the presence of any oxide precursor or any additional treatment to form the nanoparticulate film. As electrodes for dye solar cells (DSCs), the 1–3 μm-thick films modified with Dyesol N3 dye showed high photovoltaic responses, a maximum overall energy conversion efficiency of 2.4–2.5% being measured under AM1.5 illumination at 100 and 140 mW cm^{-2}. This method was extended to other semi-conducting oxides such as SnO_2. Efficiencies as high as 1.8% and 1.5% were measured under AM1.5 illumination at 64 and 140 mW cm^{-2}, respectively. This approach draws new prospects in the field of plastic organic–inorganic hybrid devices.

1. Introduction

The unique chemical, optical, electronic and/or magnetic properties of semi-conducting oxide materials associated with the remarkable features gained at the nanometer scale have stimulated extensive efforts in the preparation of nanostructured nanoporous oxide semi-conductors over the past decade. In this context, titanium dioxide (TiO_2) is one of the most important functional transition metal materials for technological and industrial purposes owing to its low-cost, chemical resistance, hardness, and environmental compatibility. Nanocrystalline TiO_2 has therefore been widely used in a broad range of important fields such as catalyst supports [1], photocatalysis [2], degradation of environmentally hazardous chemicals [3], sensors [4] and electrochromic displays [5]. Furthermore, since the breakthrough accomplished by O'Regan and Grätzel in 1991 [6], it has been well-established that dye solar cells (DSCs) based on nanoporous TiO_2 layers sensitized with polypyridyl ruthenium complexes constitute a low-cost alternative to amorphous silicon photovoltaic cells, the overall energy conversion efficiency reaching over 11% [7]. As the device performances are mainly governed by the high surface area and the controlled nanoporosity of the oxide materials employed, several methods have been developed to process suitable TiO_2 electrodes such as the classical "doctor-blade" deposition technique coupled with sintering of TiO_2 precursor pastes [8] and the "evaporation induced self-assembly" technique based on the "template" approach [9]. However, a thermal post-treatment at temperatures higher than 450 °C is generally used to achieve particle interconnection, to improve the cross-linking of the oxide and to decompose or remove traces of the organic binder or surfactant ensuring the stability of the precursor solution.

Modern portable electronic devices, i.e. mobile phones, laptops, pocket calculators or watches, require the development of renewable power sources, such as solar cells, on flexible substrates which is incompatible with a high-temperature fabrication route. In this context, various investigations have been conducted for producing nanoporous TiO_2 electrodes at temperatures lower than 150 °C for plastic DSCs, including electrophoretic deposition followed by CVD and UV-treatments to improve the connections between particles and eliminate the organic residuals respectively [10], UV-irradiation of a colloid containing nanoparticles and a metallo-organic TiO_2 precursor [11], UV-treatment followed by heating at 140–250 °C [12], hydrothermal treatment [13], chemical sintering by using an electrolyte glue [14] or a metal alkoxide [15], high frequency microwave processing [16], high power UV-laser processing [17], low-temperature sintering [18] and also high-pressure

* Corresponding author. Tel.: +33 (0)5 40 00 25 23; fax: +33 (0)5 40 00 69 94.
E-mail address: t.toupance@ism.u-bordeaux1.fr (T. Toupance).

1010-6030/$ – see front matter © 2009 Elsevier B.V. All rights reserved.
doi:10.1016/j.jphotochem.2009.03.020

compression methods [19]. Recently, the compression route led to promising results, with an overall conversion yield reaching 7.4% on ITO/plastic. Nonetheless, there is still a strong need for the development of new direct low-temperature processing methods for semi-conducting oxides.

Recently, we described a facile and direct method to fabricate anatase TiO_2 nanoporous thin films (thickness <1 μm) at low temperature for plastic electrochromic devices [20]. It involves the UV-treatment of thin TiO_2 layers prepared by the "doctor-blade" technique from TiO_2 nanoparticle-based colloids by using a cheap high-pressure mercury lamp. This method has some obvious advantages: (i) the process is simple, fast and cheap; (ii) large surface areas can be treated; (iii) no additional treatment, such as further heating, and no oxide precursors are required as in the other methods employing UV-irradiation reported so far.

We herein report on the generalization of this approach to the preparation of thicker anatase TiO_2 porous films for photovoltaic applications. The photoelectrochemical performances of the cells built with these films are compared with those obtained under similar experimental conditions after annealing at high temperature. Preliminary results concerning the extension of this method to tin dioxide (SnO_2) based systems are also reported.

2. Experimental

2.1. Materials

Titanium dioxide nanoparticles were synthesized according to a hydrothermal route adapted from a literature procedure [21] and their characterization has been reported elsewhere [20]. Triton X-100 (Aldrich), pentan-2,4-dione (Lancaster), acetic acid (Lancaster), 4-*tert*-butylpyridine (Fluka), iodine (Alfa Aesar), lithium iodide (Aldrich), propan-2-ol (Acros organics), propylene carbonate (Alfa Aesar) and bis(isothiocyanato)ruthenium(II)-bis-2,2′-bipyridine-4,4′-dicarboxylic acid (hereafter named N3, Dyesol) were used without any further purification. Large light-scattering TiO_2 (−325 mesh, Aldrich) or SnO_2 (−325 mesh, Aldrich) particles and commercial TiO_2 (T-LALT Solaronix) or SnO_2 (Alfa Aesar) colloids were used as supplied. P25 TiO_2 nanoparticles were provided by Degussa. The F-doped SnO_2/glass (10 Ω/square) and ITO/PET (70 Ω/square) transparent conductive substrates were purchased from Solems and Bekaert, respectively.

2.2. Preparation of the semi-conducting oxide porous films

Typical colloids containing hydrothermal TiO_2 nanoparticles were prepared as previously reported. The water content of the colloids enables to tune the film thickness. For instance, 5 and 3 g of water led to 1.1 and 2.3 μm-thick films, respectively. Light-scattering particles were also employed to increase the thickness and the porosity of the films. The corresponding precursor colloids were composed of 0.5 g of the above-prepared TiO_2 nanoparticles, 0.24 g of TiO_2 −325 mesh, 0.8 mL of pentan-2,4-dione, six drops of Triton X-100, and deionised water. The transparent conductive substrates were cleaned by sonication in propan-2-ol followed by UV-irradiation in air. The colloids were spread over the conductive substrates with a glass rod between single strips of 3 M Magic Tape (thickness of 40 μm) placed along the substrate edges. The conductive slides were cleaned by sonication in isopropanol followed by UV-irradiation in air. The films were then exposed for 3 h to UV-irradiation (Philips HPL-N lamp, 125 W), and, for comparison, layers on FTO/glass were sintered in air for 30 min at 450 °C. A similar procedure was employed to prepare porous electrodes based on commercial SnO_2 and commercial TiO_2 nanoparticles.

2.3. Sample characterization

The SEM and HR-SEM observations were carried out with a JEOL JSM-840A and a JEOL JSM-6700F microscope, respectively. Thickness measurements were performed with a KLA Tencor, Alfa-step IQ, profilometer. Nitrogen sorption (BET) and mercury intrusion analyses were carried out with Micromeritics ASAP 2010 and Micromeritics AutoPore IV porosimeters, either on powder or on large quantities (≈100 mg) of films scraped off the substrate. X-ray diffraction patterns were recorded on a θ/θ Bragg–Brentano X'pert MPD diffractometer (Cu Kα1+2 radiations) equipped with an X'celerator detector. The diffractograms were refined with the Fullprof software, the crystallite sizes were determined with the Scherrer relation [22] and the phase proportions with the weighted peak areas [23]. The ultra-violet–visible (UV–vis) absorption/diffuse reflectance spectra were measured with a Jasco V-560 PC spectrometer using $BaSO_4$ as the reference material. The fundamental absorption was used to determine the value of the optical band-gap. The energy gap was thus estimated using the following equation for a direct gap semi-conductor:

$$\alpha = K(h\nu - E_g)^{1/2}$$

where α is the absorption coefficient, K is a constant, and E_g is the energy gap, respectively. The energy gap was determined by extrapolating the linear portion of the plot $(\alpha h\nu)^2$ vs the energy to zero absorption [24]. The photoluminescence was recorded at 12 K using a 1 m spectrometer (1704 SPEX Czerny-Turner) fitted with a 1200 grooves/mm grating blazed at 500 nm coupled to a photomultiplier (RCA C31034). The spectra were collected at 90° using a *c.w.* He–Cd laser (325 nm) as the excitation source. The contact angles with water were determined with a DSA100, Krüss.

2.4. Cell fabrication and photoelectrochemical measurements

Sensitization of the photoelectrodes with the N3 dye was achieved by immersing the electrodes in a 2.5 mM solution of dye in dry ethanol at RT for 48 h. The amount of chemisorbed dye was estimated by UV–vis spectrometry at 530 nm with a Hewlett Packard 8453 spectrophotometer. A 40-μm spacer with a hole in the middle was stuck onto a Pt-sputtered FTO/glass counter-electrode. The electrolyte (0.5 M LiI, 0.05 M iodine, 0.5 M 4-*tert*-butylpyridine in propylene carbonate) was deposited on the bare part and the dye-sensitized electrode was placed on top. An aluminum device with screws held the two components of the cell together delimiting an active area of about 0.2 cm^2. An Xe solar simulator (AM1.5) calibrated with a radiometer (IL 1400BL) was used to illuminate the cell between 64 and 180 mW cm^{-2} and the *I–V* responses were measured with a Keithley 4200. The IPCE values were collected every nanometer from 300 to 1000 nm using an Xe lamp with a monochromator (Triax 180, Jobin Yvon). The cell was illuminated without bias light. The spot size ca. 3 mm of diameter was smaller than the size of the DSC cell. The current produced was measured by steps of 1 nm after 200 ms of radiation exposure with a Keithley 6487 picoammeter. The incident photon flux was measured with a 6-in. diameter calibrated integrated sphere with a silicon detector.

3. Results and discussion

3.1. Thin film characterization

A fine control of the TiO_2 concentration in the colloidal precursor enables to vary the film thickness in the 1.1–2.3 μm range and the addition of light-scattering particles (average diameter 40–200 nm) enables to reach values as high as 5 μm (Fig. 1). In each case, UV-irradiation in air for 3 h leads to the formation of

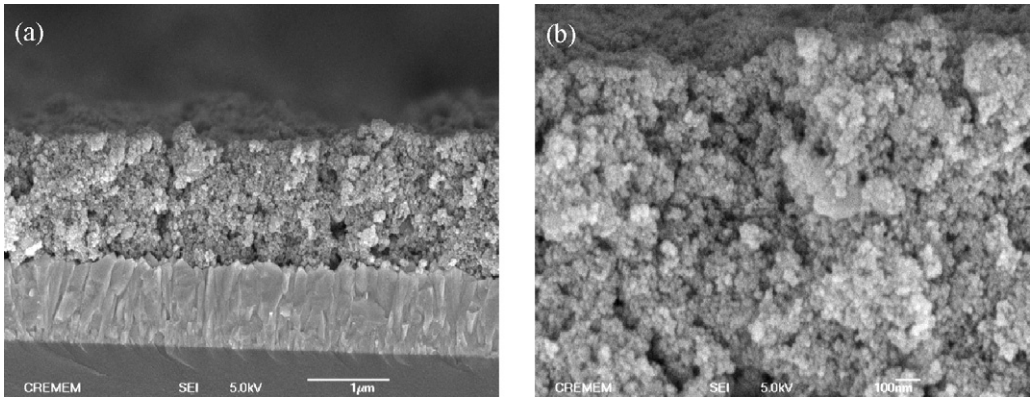

Fig. 1. SEM images of UV-processed TiO_2 films made from hydrothermal TiO_2 nanoparticles with light-scattering particles. Substrate: FTO–glass.

porous crack-free films made of aggregated nanoparticles with no preferential orientation showing the same composition as the powder, i.e. anatase/brookite: 9/1. To highlight the effect of the UV-treatment on the textural and optical properties, a large number of films were scraped off and studied by nitrogen sorption and mercury intrusion porosimetries, and by UV–vis absorption and photoluminescence spectroscopies. The layers prepared from the hydrothermal TiO_2 nanoparticles with or without light-scattering particles show the same porosity and BET surface areas as the starting particles, respectively 74 and 100 $m^2\,g^{-1}$. In contrast, a thermal treatment at 450 °C leads to a noteworthy decrease of these values, i.e. 64 and 89 $m^2\,g^{-1}$. As previously reported [20], the complete decomposition of the organics by the UV-treatment was evidenced by TGA analyses. As a result, UV-irradiation in air enables the preparation of organic free porous films with no sintering or densification action. On the other hand, the energy band-gap values estimated for untreated TiO_2, HT-treated TiO_2, and UV-treated TiO_2 nanoparticles are around 3.25 eV (Fig. 2). These values are typical of bulk anatase (3.2 eV) [25] indicating that there is no quantum confinement and that the different treatments do not significantly change the electronic structure. No brookite contribution, expected around 3.1 eV [26], was detected which might be explained by the crystallite size smaller than 10 nm leading to an absorption edge higher than 3.2 eV. Regardless of the post-treatment employed, the low-temperature steady-state photoluminescence spectra exhibits a main large and broad emission band between 400 and 600 nm with a maximum around 530 nm (2.34 eV) along with a low-intensity contribution around 400 nm (3.1 eV). The main emission

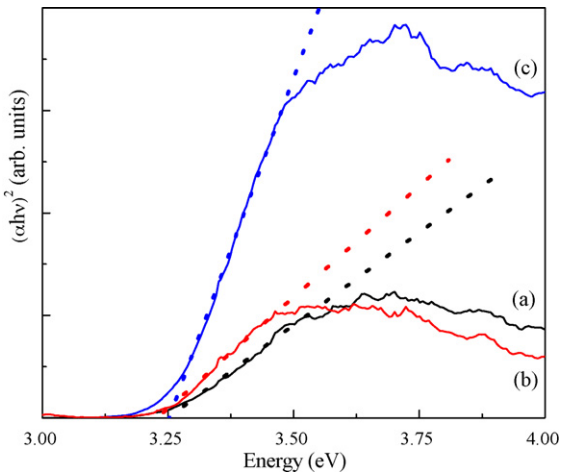

Fig. 2. $\alpha h\nu^2$ vs energy ($h\nu$) plots for the (a) as-prepared TiO_2, (b) HT-treated TiO_2 and (c) UV-treated TiO_2. The dotted lines correspond to data best linear fit.

component can be ascribed to the presence of surface trap states or oxygen-related defects, and transitions of electrons from the conduction band edge to holes, trapped at interstitial Ti^{3+} sites, respectively [27], whereas the origin of the higher energy component is not known exactly. It may involve phonon-assisted indirect transitions between the conduction and the valence band [28]. Finally, the contact angles of the UV- and HT-processed layers with water were determined. A lower value, i.e. 5°, was measured for the UV-treated films than for the HT films, i.e. 26°, which reveals the higher hydrophilic nature of the former films. This behavior can be related to a hydroxylation of the oxide surface. It is indeed well-known that UV-irradiation strongly improves the hydrophilicity of TiO_2 thin film surface [29]. Thus, a plausible mechanism involves the formation of oxygen vacancies upon irradiation [30] that favour the dissociative adsorption of water molecules providing surface hydroxyl groups under air [31].

This approach was also extended to other metal oxides such as SnO_2. Thus, UV-processed SnO_2 thin films were prepared by the same method from colloids containing both SnO_2 nanoparticles (5 nm) and light-scattering particles (0.2 μm). As for TiO_2, crack-free porous films were obtained, the structure and the morphology of which were comparable to those of the starting dried colloid. The film thickness was varied in the range from 1.3 to 3.3 μm depending on the concentration of the colloid.

3.2. Photoelectrochemical behavior of TiO_2-based cells

After reaction with the N3 dye to sensitize the oxide layers, the photovoltaic performances of the UV-treated TiO_2 films were investigated under AM1.5 irradiation (140 mW cm^{-2}) using a standard iodide–iodine based liquid electrolyte and compared to that of commercial TiO_2 nanoparticles and high-temperature processed layers. The photovoltaic data, summarized in Table 1, reveals that the UV-treatment in air method yields films that show performances, for thin films, higher than the high-temperature treated ones. Thus, for a 1.1 μm-thick film, the overall efficiency reaches 1.4% whereas the same film sintered at 450 °C shows only a 1.2% efficiency owing to lower open-circuit voltage (V_{oc}) and fill factor (FF) values. Fabrication of thicker UV-processed films from the hydrothermal TiO_2 nanoparticles led to a slight increase of the energy conversion yield, a plateau value of 1.6% being reached for a 2.3 μm film. The performances are limited by the short-circuit current density which only slightly increases with the film thickness (from 4.4 to 4.8 mA cm^{-2} for 1.1 and 2.3 μm-thick films, respectively). The short-circuit current density (J_{sc}) is determined by the external quantum efficiency, which is the product of the light harvesting efficiency, the electron injection efficiency and the electron collection efficiency [32]. In our systems, the light harvesting efficiency appears not to be an issue.

Table 1
Comparison of the photovoltaic performance of the DSCs based on electrodes made from hydrothermal TiO_2 nanoparticles. Active surface area: 0.2 cm^2; illumination: AM1.5 140 mW cm^{-2}; th: film thickness; J_{sc}: short-circuit photocurrent density; V_{oc}: open-circuit photovoltage; FF: fill factor; Eff.: overall efficiency.

Precursor[a]	Conditions[b]	th (μm)	J_{sc} (mA cm^{-2})	V_{oc} (V)	FF	Eff. (%)
Oxide 1	UV	1.1	4.4	0.78	0.59	1.4
Oxide 1	UV	2.3	4.8	0.75	0.62	1.6
Oxide 1	HT	1.1	4.3	0.71	0.54	1.2
Oxide 1	HT	2.3	6.3	0.63	0.57	1.6
Oxide 2	UV	1.4	6.1	0.79	0.63	2.2
Oxide 2	UV	2.0	7.0	0.77	0.63	2.4
Oxide 2	UV	2.4	6.7	0.76	0.64	2.3
Oxide 2	UV	2.7	6.7	0.77	0.64	2.4
Oxide 2	UV	2.9	6.7	0.76	0.66	2.4
Oxide 2	UV	3.7	7.0	0.76	0.63	2.4
Oxide 2	UV	3.8	7.2	0.77	0.62	2.5
Oxide 2	HT	2.9	7.7	0.70	0.53	2.0

[a] Oxide 1: hydrothermal TiO_2 nanoparticles; oxide 2: hydrothermal TiO_2 nanoparticles + light-scattering TiO_2 particles (Aldrich).
[b] UV: UV-irradiation – HPL-N lamp 125 W for 3 h; HT: 450 °C for 30 min.

Indeed, the optical absorption of the dye-modified porous electrode increases almost linearly with the film thickness (from 0.4 to 0.8 at 530 nm for 1.1 and 2.3 μm-thick films, respectively), evidencing that the dye penetrates into the whole film. When, the parameters related to the collection efficiency are studied, it appears that the short-circuit current density almost linearly increases when the illumination is varied from 70 to 175 mW cm^{-2} (Fig. 3A), revealing that the current is not limited by small necking between the particles, that could limit the electron density passing through the necks. A UV-irradiation from underneath produces the same results as that from above the films. When the films are irradiated at the same time from underneath and above, similar photovoltaic responses are also obtained. This indicates that the short-circuit current density plateau is not related to a UV penetration issue. Furthermore, to investigate the electron diffusion length, the performances of the cells were measured by illuminating them through the TiO_2 layer side and from the counter-electrode side. The performances were expected to decrease when the cell was illuminated from the counter-electrode side due to the absorption of the electrolyte and the reflexion of the platinum. The J_{sc} decreased by around 30% for cells made of 1.1 and 2.3 μm-thick films that were UV-treated or sintered at 450 °C. This shows that there is therefore no electron diffusion length issue, since, if there was, the performances of the cell with a 2.3 μm-thick UV-treated film illuminated from the counter-electrode side would have decreased by much more than 30% due to absorption of the outer layer that would not contribute to the J_{sc}. As a consequence, these results suggest that the optimum thickness is slightly higher than 1.1 μm and that a poor mediator diffusion into the pores of the thicker films affects the dye regeneration near the FTO/TiO_2 interface and is at the origin of the J_{sc} plateau value observed. This phenomenon is consistent with the linear dependence of the J_{sc} with the illumination intensity. Indeed, the iodine concentration gradient increases with the light intensity which raises the diffusion rate and enables the J_{sc} to increase. In contrast, the J_{sc} of HT films increases with the film thickness, which could be related to larger pores, i.e. 15 nm for HT films instead of 12 nm for UV films according to mercury intrusion porosimetry measurements. It must also be noted that the optical absorption is lower for the HT films (0.3 and 0.6 at 530 nm for 1.1 and 2.3 μm-thick films, respectively). This could be due partly to the lower surface area of the HT films but also to enhanced dye uptake due to more hydroxyl groups induced by the UV-treatment [33].

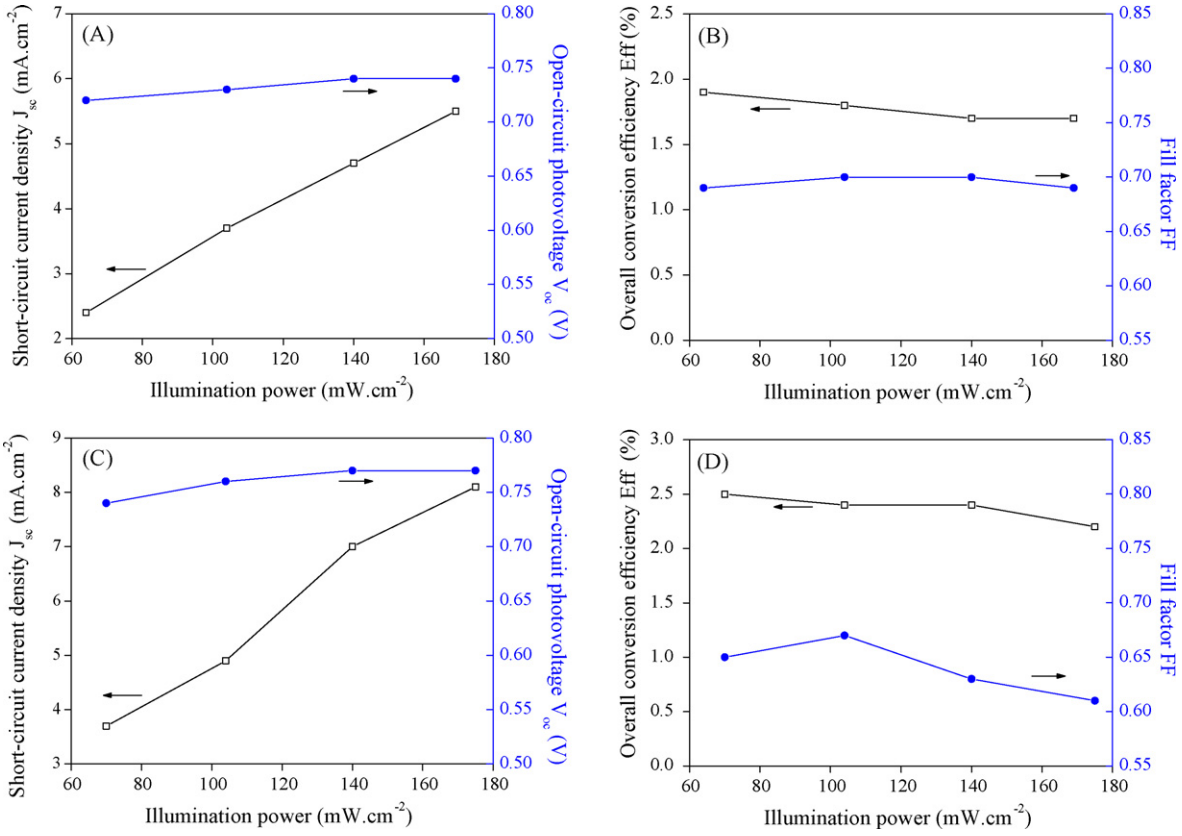

Fig. 3. Evolution of the short-circuit current density (J_{sc}), open-circuit photovoltage (V_{oc}), fill factor (FF) and overall conversion efficiency (eff.) as a function of the illumination power for DSCs based on a N3-sensitized TiO_2 film prepared from (A, B) hydrothermal TiO_2 nanoparticles (2.3 μm-thick), and (C, D) hydrothermal nanoparticles in the presence of light-scattering TiO_2 particles (2.0 μm-thick). The measurements were performed under AM1.5 illumination.

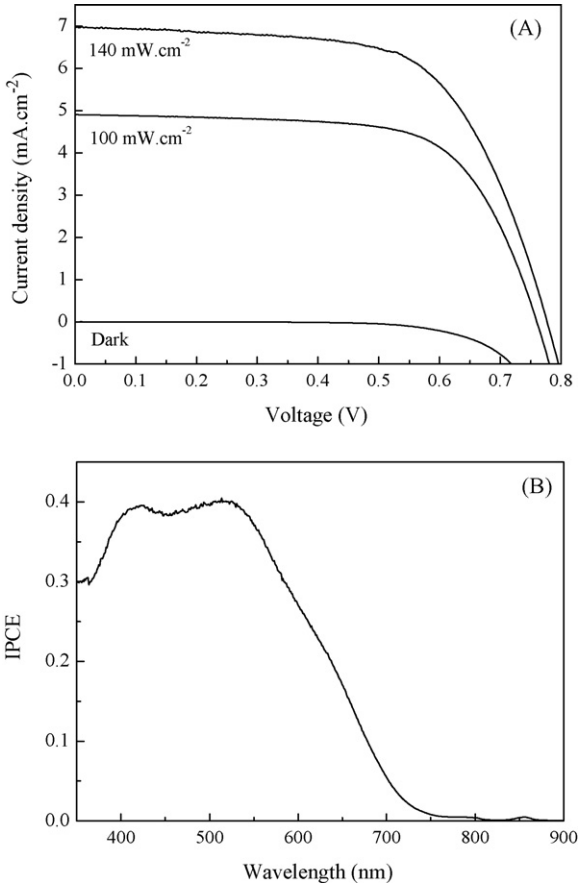

Fig. 4. (A) Current–voltage curves in the dark (lower curve) and under AM1.5 illumination at 140 mW cm^{-2} and 100 mW cm^{-2} (upper curves) for a DSC based on a N3-sensitized 2.9 μm thick TiO_2 film prepared from hydrothermal TiO_2 nanoparticles in the presence of light-scattering TiO_2 particles. (B) Incident photon-to-current efficiency (IPCE) of the previous cell.

To highlight the influence of the porosity on the photovoltaic performances, the film thickness and the pore size were varied by adding large light-scattering TiO_2 particles, i.e. 40–200 nm, to the hydrothermal TiO_2 nanoparticles. A typical *I–V* curve is depicted in Fig. 4A for a 2.9 μm-thick film on FTO with a J_{sc} of 6.7 mA cm^{-2}, a V_{oc} of 0.76 V and a FF of 0.66 corresponding to an overall energy conversion efficiency of 2.4%. As for films prepared from nanoparticles only, the J_{sc} value increases linearly with the illumination power whereas the conversion yield remains almost unchanged (Fig. 3C and D). In addition, the incident photon-to-current efficiency (IPCE) plot shows a maximum quantum yield of 40% for the 400–600 nm wavelength region (Fig. 4B) which falls into the range of the one reported for films prepared at low temperature by chemical sintering [14]. The current also reaches a plateau around 7 mA cm^{-2}, suggesting an optimum thickness for these films around 2 μm which is higher than that found for the films without light-scattering particles. We also assessed using this low-temperature method for preparing nanoporous TiO_2 films on ITO/PET substrates. In this case, the solar energy conversion efficiency reaches 1.8% for a 3.0 μm-thick film with a J_{sc} of 5.7 mA cm^{-2}, a V_{oc} of 0.76 V and a FF of 0.57.

The exact UV effect was assessed, since the temperature can go up to 80 °C during the UV-irradiation, the photovoltaic response of a film containing light-scattering particles treated at 150 °C for 3 h was tested. The corresponding efficiency is then very low, i.e. 0.5% compared to 2.4%, which unambiguously demonstrates that the UV-irradiation in air actually interconnects the particles, either through the direct effect of the UV light or that of the ozone generated by the UV light in the air. One may argue that the low efficiency is due to the organic residuals not eliminated at 150 °C, but they are not a limiting factor since, as evidenced below, the compressed films made from the colloid containing light-scattering particles and organics, which are not eliminated, provide reasonable performances. Since TiO_2 strongly absorbs UV-irradiation, it seems more likely that the particle connexion is obtained through the effect of the created ozone. 1.1 μm-thick films of hydrothermal TiO_2 nanoparticles were exposed to an ozone/air atmosphere or to UV-irradiation in a reactor under a nitrogen flux. It appears that the performances go down by around 50% for the different cells (Table 2), indicating that the particle connexion results from the combination of the action of the ozone and of UV-irradiation. The low open-circuit potential obtained for the cell with a UV/nitrogen treated film shows that the ozone is at the origin of the high open-circuit potentials observed for the low-temperature processed films.

In order to clarify the origin of the photocurrent limitations evidenced above, UV-processed films made from commercial P25 and Solaronix TiO_2 colloids were characterized (Table 3). They led to lower efficiencies, the J_{sc} value reaching a plateau for a given thickness, i.e. around 3 μm for P25. This underlines that the as-prepared hydrothermal nanoparticles are not the limiting component. One must note the higher performances of the Solaronix colloid when treated by UVs instead of at 130 °C, the temperature for which the colloid is designed. On the other hand, DSCs built with films compressed statically at 660 MPa also show a current plateau revealing that the UV-treatment is not the limiting factor either. This behavior is in agreement with recent reports showing that small pore sizes, due to the use of small nanoparticles and to the fact that no binder is fired to create larger cavities, limit the current by ham-

Table 2
Effect of the atmosphere and treatment on the performances of 1.1 μm-thick films made of hydrothermal TiO_2 nanoparticles. Active surface area: 0.2 cm^2; illumination: 140 mW cm^{-2}; J_{sc}: short-circuit photocurrent density; V_{oc}: open-circuit photovoltage; FF: fill factor; Eff.: overall efficiency.

Treatment	J_{sc} (mA cm^{-2})	V_{oc} (V)	FF	Eff. (%)
Ozone/air	2.2	0.77	0.63	0.8
Control film UV/air	4.0	0.79	0.64	1.4
UV/nitrogen	2.2	0.66	0.57	0.6
Control film UV/air	3.4	0.74	0.63	1.1

Table 3
Comparison of the photovoltaic performance of the DSCs based on electrodes fabricated by UV-irradiation from commercial TiO_2 nanoparticles. Active surface area: 0.2 cm^2; illumination: AM1.5 140 mW cm^{-2}; th: film thickness; J_{sc}: short-circuit photocurrent density; V_{oc}: open-circuit photovoltage; FF: fill factor; Eff.: overall efficiency.

Precursor[a]	Conditions[b]	th (μm)	J_{sc} (mA cm^{-2})	V_{oc} (V)	FF	Eff. (%)
Aldrich TiO_2	UV	1.0	0.7	0.76	0.60	0.2
Aldrich TiO_2	UV	2.0	1.0	0.75	0.62	0.3
Aldrich TiO_2	UV	3.5	1.4	0.76	0.61	0.5
P25 TiO_2	UV	1.6	3.0	0.76	0.63	1.0
P25 TiO_2	UV	2.3	3.9	0.76	0.64	1.4
P25 TiO_2	UV	3.0	4.2	0.75	0.68	1.5
P25 TiO_2	UV	3.9	4.3	0.75	0.68	1.6
Solaronix	130 °C	2.3	4.3	0.69	0.64	1.4
Solaronix	UV	2.3	6.1	0.68	0.62	1.8
Solaronix	UV	4.8	5.5	0.65	0.65	1.7
Oxide 2	660 MPa	1.6	5.1	0.76	0.60	1.7
Oxide 2	660 MPa	2.3	5.0	0.76	0.59	1.6

[a] Aldrich TiO_2: light-scattering particles; P25: commercial TiO_2 from Degussa; Solaronix: commercial T-LALT colloid designed for sintering at 130 °C; oxide 2: hydrothermal TiO_2 nanoparticles + light-scattering TiO_2 particles (Aldrich).

[b] UV: UV-irradiation – HPL-N lamp 125 W for 3 h; 130 °C: annealed in air at 130 °C for 24 h; 660 MPa: compressed at 660 MPa.

Table 4
Effect of a 3-week aging between the UV-treatment and the dye-adsorption on the photovoltaic performance of the DSCs based on TiO_2 particles. Active surface area: 0.2 cm^2; illumination: AM1.5 140 mW cm^{-2}; th: film thickness; J_{sc}: short-circuit photocurrent density; V_{oc}: open-circuit photovoltage; FF: fill factor; Eff.: overall efficiency; oxide 1: as-prepared hydrothermal TiO_2 nanoparticles; oxide 2: hydrothermal TiO_2 nanoparticles + light-scattering TiO_2 particles (Aldrich).

Precursor[a]	Conditions[b]	J_{sc} (mA cm^{-2})	V_{oc} (V)	FF	Eff. (%)
Oxide 1	UV	3.1	0.76	0.67	1.1
Oxide 1	UV then 3 weeks aging	2.6	0.72	0.66	0.9
Oxide 2	UV	4.8	0.79	0.64	1.8
Oxide 2	UV then 3 weeks aging	3.8	0.75	0.65	1.3

pering the diffusion of the redox mediator [34]. This hypothesis is reinforced by the fact that, at least up to 3.5 μm, no current saturation is observed when UV-processed films composed of only the large light-scattering TiO_2 particles are tested (Table 3).

The open-circuit voltages and fill factors measured for the layers made of the hydrothermal TiO_2 nanoparticles, in the presence or not of light-scattering particles, by UV-irradiation in the air are higher than those of the corresponding HT films. This may be caused by a shift of the Fermi level toward the bottom of the conduction band and a decrease of the recombination phenomena. It is also evidenced by the weak dependence of the efficiency upon the illumination power (Fig. 3B–D). Moreover, according to contact angle measurements, the higher V_{oc} values for UV-processed films probably arise from more hydroxylated anatase nanoparticles leading to less recombinations, i.e. higher electron life time, and a shift of the Fermi level. It is also worthwhile to mention that a significant decrease of the photovoltaic performances was noted when the films were aged several weeks in a dessicator before N3 adsorption and photovoltaic measurements. In this case, both J_{sc} and V_{oc} decrease due to a less hydroxylated film as evidenced by the increase of the contact angle of the TiO_2 photoelectrode with water (5–30°) (Table 4). This result underlines the positive effect of the UV-irradiation under air.

3.3. Photoelectrochemical behavior of SnO_2-based cells

Photoelectrochemical measurements were also performed on N3-modified SnO_2 layers (Table 5). The corresponding results reveal that efficiencies as high as 1.5% can be reached for a 3.3 μm-thick film at 140 mW cm^{-2}, which is 50% higher than that determined for high-temperature annealed films, owing to higher fill factor (0.50 to be compared with 0.37) and open-circuit photovoltage (0.53 V to be compared with 0.46 V) as depicted in Fig. 5. Moreover, the energy conversion efficiency is even better at lower light intensity since a value of 1.8% was measured at 64 mW cm^{-2}. On ITO/PET substrates, the conversion efficiency reaches 0.9% for a 3.3 μm-thick SnO_2 film with a J_{sc} of 4.9 mA cm^{-2}, a V_{oc} of 0.55 V and a FF of 0.47. These results are therefore very promising since the efficiencies reported for high-temperature processed SnO_2-based DSCs rarely exceed 1.3% [35]. The evolution of the photovoltaic performances

Table 5
Comparison of the photovoltaic performance of the DSCs based on SnO_2 electrodes fabricated by UV and HT sintering. Film thickness: 3.3 μm; active surface area: 0.2 cm^2; J_{sc}: short-circuit photocurrent density; V_{oc}: open-circuit photovoltage; FF: fill factor; Eff.: overall efficiency.

Film[a]	Illumination power (mW cm^{-2})	J_{sc} (mA cm^{-2})	V_{oc} (V)	FF	Eff. (%)
UV-SnO_2	64	4.2	0.51	0.54	1.8
UV-SnO_2	140	7.8	0.53	0.50	1.5
HT-SnO_2	140	8.2	0.46	0.37	1.0

[a] Precursor: Alfa Aesar SnO_2 colloid + large scattering SnO_2 nanoparticles (Aldrich); UV: UV-irradiation: HPL-N lamp 125 W for 3 h; HT: 450 °C for 30 min.

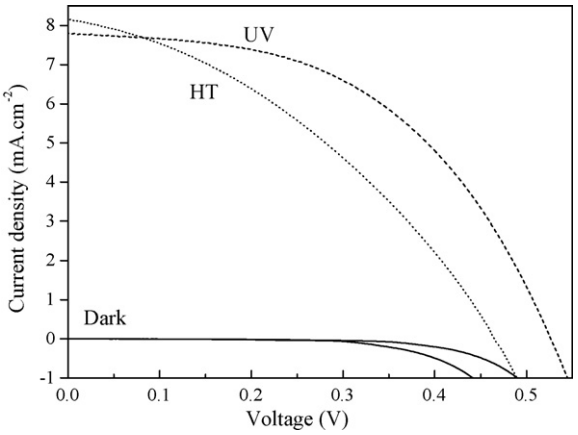

Fig. 5. Current–voltage curves in the dark and under AM1.5 illumination at 140 mW cm^{-2} for a DSC based on a N3-sensitized 3.3 μm SnO_2 film prepared from commercial Alfa Aesar nanoparticles in the presence of light-scattering SnO_2 particles (Aldrich) after thermal treatment at 450 °C (dotted line) or UV-irradiation (dashed line).

Table 6
Comparison of the photovoltaic performance of the SnO_2-based DSSCs processed by UV and HT as a function of the illumination power. Film thickness: 2.2 μm; active surface area: 0.2 cm^2; J_{sc}: short-circuit photocurrent density; V_{oc}: open-circuit photovoltage; FF: fill factor; Eff.: overall efficiency.

Film[a]	Illumination power (mW cm^{-2})	J_{sc} (mA cm^{-2})	V_{oc} (V)	FF	Eff. (%)
UV-SnO_2	72	2.8	0.47	0.51	0.92
UV-SnO_2	97	3.7	0.48	0.50	0.90
UV-SnO_2	140	5.3	0.49	0.47	0.88
UV-SnO_2	178	7.3	0.50	0.43	0.88
HT-SnO_2	72	2.7	0.42	0.37	0.57
HT-SnO_2	97	3.7	0.44	0.35	0.58
HT-SnO_2	140	5.0	0.45	0.33	0.52
HT-SnO_2	178	6.1	0.46	0.31	0.49

[a] Precursor: Alfa Aesar SnO_2 colloid + large scattering SnO_2 nanoparticles (Aldrich); UV: UV-irradiation – HPL-N lamp 125 W for 3 h; HT: 450 °C for 30 min.

of UV- and HT-treated SnO_2 cells with the illumination power was studied for a film thickness of about 2.2 μm (Table 6). In contrast to TiO_2 films for which the results are quite stable with the light power, the higher the illumination power, the lower the performances of the HT-treated films indicate high recombination rates. This behavior is fully consistent with the studies of charge transport and recombination in DSCs using TiO_2 and SnO_2 films showing that recombination rates are several orders of magnitude higher with the latter oxide than with the former [36]. Nonetheless, our results demonstrate that this phenomenon is less marked in the case of UV-processed films. Consequently, this treatment effectively decreases the recombination rate [37].

4. Concluding remarks

We have successfully developed a very simple, straightforward and cheap method for processing low-temperature anatase TiO_2 porous films in the 1–3 μm thickness range by a direct UV-irradiation in air without any additional treatment or oxide precursor. The 1–3 μm-thick films show high photovoltaic responses, a maximum overall energy conversion efficiency of 2.5% being measured under AM1.5 at 140 mW cm^{-2}. For each oxide precursor studied, an optimum film thickness was evidenced due to small pore size leading to low diffusion of the mediator when the films are too thick. This route provides better performances than the high temperature one when the film thickness is low, i.e. 1.1 and 2.0 μm for films made of TiO_2 nanoparticles and nanoparticles plus

light-scattering particles, respectively. Our results show that particle interconnexion can be obtained by UV-irradiation in air and suggest that the UV-processed films possess more surface hydroxyl groups that enhance dye-adsorption, shift the conduction band upwards and limit the recombinations. This method was generalized to tin dioxide porous films for which the beneficial effect of the UV-treatment plays a key role to diminish the recombination rate.

In contrast to previous works which always associate an additional treatment to the UV-treatment [11], our experimental results are the first demonstration of the role of the UV-treatment in air to connect oxide particles and such a finding should find valuable developments for other oxides and applications in photocatalysis or chemical sensors.

Acknowledgments

Mrs Elisabeth Sellier (University of Bordeaux 1), Rute A.S. Ferreira and M.M. Peres (Universidade de Aveiro) are acknowledged for their precious assistance. The authors wish to thank the CNRS, the Aquitaine Region (ZT PhD fellowship), the "Agence Nationale de la Recherche" (contract no. ANR-05-PV-008-14), the European Community (FAME network of Excellence) and Du Pont (USA) for partial support of this work.

References

[1] J.D. Stiehl, T.S. Kim, S.M. McClure, C.B. Mullins, J. Am. Chem. Soc. 126 (2004) 1606–1607;
M. Boronat, P. Concepcion, A. Corma, S. Gonzales, F. Illas, P. Serna, J. Am. Chem. Soc. 129 (2007) 16230–16237.
[2] J. Zhang, Y. Hu, M. Matsuoka, H. Yamashita, M. Minagawa, H. Hidaka, M. Anpo, J. Phys. Chem. B 105 (2001) 8395–8398;
M.S. Hamdy, O. Berg, J.C. Jansen, T. Maschmeyer, J.A. Moulijn, G. Mul, Chem. Eur. J. 12 (2006) 620–628;
S. Shanmugam, A. Gabashvili, D.S. Jacob, J.C. Yu, A. Gedanken, Chem. Mater. 18 (2006) 2275–2282.
[3] M.R. Hoffmann, S.T. Martin, W. Choi, D. Bahnemann, Chem. Rev. 95 (1995) 69–96;
F. Fresno, C. Guillard, E. Coronado, J.M. Chovelon, D. Tuleda, J. Soria, J.-M. Hermann, J. Photochem. Photobiol. A: Chem. 173 (2005) 13–20.
[4] E. Palomares, R. Vilar, A. Green, R. Durrant, Adv. Funct. Mater. 14 (2004) 111–115;
E. Coronado, J.R. Galan-Mascaros, C. Marti-Gastaldo, E. Palomares, J.R. Durrant, R. Vilar, M. Grätzel, Md.K. Nazeeruddin, J. Am. Chem. Soc. 127 (2005) 12351–12356.
[5] K.W. Park, Inorg. Chem. 44 (2005) 3190–3193;
G. De Filpo, F.P. Nicoletta, Chidichimo, Chem. Mater. 18 (2006) 4662–4666.
[6] B. O'Regan, M. Grätzel, Nature 353 (1991) 737–740.
[7] M. Grätzel, J. Photochem, Photobiol. A: Chem. 164 (2004) 3–14;
Md.K. Nazeeruddin, F. De Angelis, S. Fantacci, A. Selloni, G. Viscardi, P. Liska, S. Ito, B. Takeru, M. Grätzel, J. Am. Chem. Soc. 127 (2005) 16835–16847.
[8] Md.K. Nazeeruddin, A. Kay, I. Rodicio, R. Humphry-Baker, E. Müller, P. Liska, N. Vlachopoulos, M. Grätzel, J. Am. Chem. Soc. 115 (1993) 6382–6390.
[9] B. Smarsly, D. Grosso, T. Brezesinski, N. Pinna, C. Boissière, M. Antonietti, C. Sanchez, Chem. Mater. 16 (2004) 2948–2952;
E. Lancelle-Beltran, P. Prené, C. Boscher, P. Belleville, P. Buvat, C. Sanchez, Adv. Mater. 18 (2006) 2579–2582;
E. Lancelle-Beltran, P. Prené, C. Boscher, P. Belleville, P. Buvat, S. Lambert, F. Guillet, C. Boissière, D. Grosso, C. Sanchez, Chem. Mater. 18 (2006) 6152–6156.
[10] T.N. Murakami, Y. Kijitori, N. Kawashima, T. Miyasaka, J. Photochem, Photobiol. A: Chem. 164 (2004) 187–191.
[11] D. Gutierrez-Tauste, I. Zumeta, E. Vigil, M.A. Hernandez-Fenollosa, X. Domenech, J.A. Ayllon, J. Photochem. Photobiol. A: Chem. 175 (2005) 165–171;
D. Zhang, T. Yoshida, G. Oekermann, K. Furuta, H. Minoura, Adv. Funct. Mater. 16 (2006) 1228–1234.
[12] C. Longo, J. Freitas, M.A. DePaoli, J. Photochem, Photobiol. A: Chem. 159 (2003) 33–39;
L.N. Lewis, J.L. Spivack, S. Gasaway, E.D. Williams, J.Y. Gui, V. Manivannan, O.P. Siclovan, Sol. Energy Mater. Sol. Cells 90 (2006) 1041–1051.
[13] D. Zhang, T. Yoshida, K. Furuta, H. Minoura, J. Photochem. Photobiol. A: Chem. 164 (2004) 159–166.
[14] N.-G. Park, K.M. Kim, M.G. Kang, K.S. Ryu, S.H. Chang, Y.-Y. Shin, Adv. Mater. 17 (2005) 2349–2353.
[15] E. Stathatos, Y. Chen, D.D. Dionysiou, Sol. Energy Mater. Sol. Cells 92 (2008) 1358–1365.
[16] S. Uchida, M. Tomiha, H. Takizawa, M. Kawaraya, J. Photochem. Photobiol. A: Chem. 164 (2004) 93–96.
[17] H. Kim, R.C.Y. Auyeung, M. Ollinger, G.P. Kushto, Z.H. Kafafi, A. Piqué, Appl. Phys. A 83 (2006) 73–76.
[18] F. Pichot, J.R. Pitts, B.A. Gregg, Langmuir 16 (2000) 5626–5630.
[19] H. Lindström, A. Holmberg, E. Magnusson, S.-T. Lindquist, L. Malmqvist, A. Hagfeldt, Nano. Lett. 1 (2001) 97–100;
J. Halme, J. Saarinen, P. Lund, Sol. Energy Mater. Sol. Cells 90 (2006) 887–899;
T. Yamaguchi, N. Tobe, D. Matsumoto, H. Arakawa, Chem. Commun. 45 (2007) 4767–4769.
[20] O. Tebby, T. Babot, D.-H. Toupance, G. Park, M.-H. Campet, Delville, Chem. Mater. 20 (2008) 7260–7267.
[21] A. Zaban, S.T. Aruna, S. Tirosh, B.A. Gregg, Y. Mastai, J. Phys. Chem. B 104 (2000) 4130–4133.
[22] N.-G. Park, M.G. Kang, K.S. Ryu, K.M. Kim, S.H. Chang, J. Photochem. Photobiol. A: Chem. 161 (2004) 105–110.
[23] H. Zhang, J.F. Banfield, J. Phys. Chem. B 104 (2000) 3481–3487.
[24] Y. Zhao, C. Li, X. Liu, F. Gu, H. Jiang, W. Shao, L. Zhang, Y. He, Mater. Lett. 61 (2007) 79–83.
[25] H. Tang, F. Levy, H. Berger, P.E. Schmid, Phys. Rev. B 52 (1995) 7771–7774;
R. Asahi, T. Morikawa, T. Ohwaki, K. Aoki, Y. Taga, Science 293 (2001) 269–271.
[26] L.-G. Li, T. Ishigaki, X. Sun, J. Phys. Chem. C 11 (2007) 4969–4976.
[27] D. Pan, N. Zhao, Q. Wang, S. Jiang, X. Ji, Adv. Mater. 17 (2005) 1991–1995.
[28] N. Serpone, D. Lawless, R. Khairutdinov, J. Phys. Chem. 99 (1995) 16646–16654;
Y. Nakato, A. Tsumura, H. Tsubomura, Chem. Phys. Lett. 85 (1982) 387–390.
[29] N. Sakai, A. Fujishima, T. Watanabe, K. Hashimoto, J. Phys. Chem. B 105 (2001) 3023–3026;
J.C. Yu, J. Yu, H.Y. Tang, L. Zhang, J. Mater. Chem. 12 (2002) 81–85;
Y. Gao, Y. Masuda, K. Koumoto, Langmuir 20 (2004) 3188–3194;
T.L. Thompson, J.T. Yates, Chem. Rev. 106 (2006) 4428–4453.
[30] M. Miyauchi, A. Nakajima, A. Fujishima, K. Hashimoto, T. Watanabe, Chem. Mater. 12 (2000) 3–5.
[31] A. Fahmi, C. Monot, Surf. Sci. 304 (1994) 343–348.
[32] J. Halme, G. Boschloo, A. Hagfeldt, P. Lund, J. Phys. Chem. C 112 (2008) 5623–5637.
[33] F. Hirose, K. Kuribayashi, T. Suzuki, Y. Narita, Y. Kimura, M. Niwano, Electrochem. Solid-State Lett. 11 (2008) A109–A111.
[34] T. Miyasaka, M. Ikegami, K. Kijitori, J. Electrochem. Soc. 5 (2007) A455–A461.
[35] M. Kay, Grätzel, Chem. Mater. 14 (2002) 2930–2935.
[36] A.N.M. Green, E. Palomares, S.A. Haque, J.M. Kroon, J.R. Durrant, J. Phys. Chem. B 109 (2005) 12525–12533.
[37] J. Nissfolk, K. Fredin, A. Hagfeldt, G. Boschloo, J. Phys. Chem. B 110 (2006) 17715–17718.